

No-Reference Retinal Image Sharpness Metric Using Daubechies Wavelet Transform

P. Vonghirandecha¹, P. Bhurayanontachai², S. Kansomkeat¹, S. Intajag¹

¹Division of Computational Science, Faculty of Science, Prince of Songkla University, Songkhla, Thailand. (e-mail: preecha.v@psu.ac.th)

²Department of Ophthalmology, Faculty of Medicine, Prince of Songkla University, Songkhla, Thailand.

Received: March 27, 2021. Revised: August 3, 2021. Accepted: August 24, 2021. Published: August 26, 2021.

Abstract—Retinal fundus images are increasingly used by ophthalmologists both manually and without human intervention for detecting ocular diseases. Poor quality retinal images could lead to misdiagnosis or delayed treatment. Hence, a picture quality index was a crucial measure to ensure that the obtained images from acquisition system were suitable for reliable medical diagnosis.

In this paper, a no-reference retinal image quality assessment based on wavelet transform is presented. A multiresolution Daubechies (db2) wavelet at level 4 was employed to decompose an original image into detail, and approximation sub-bands for extracting the sharpness information. The sharpness quality index was calculated from the entropy of the sub-bands.

The proposed measure was validated by using images from the High-Resolution Fundus (HRF) dataset. The experimental results show that the proposed index performed more consistent with human visual perception and outperformed the Abdel-Hamid *et al* method.

Keywords—Image quality index, wavelet, entropy, retinal image.

I. INTRODUCTION

Retinal images are widely used to diagnose by ophthalmologists both with manual and without human intervention to identify and care for various eye diseases. Diagnosis accuracy is highly dependent on the quality of retinal images. The image can be degraded not only by capturing devices but also by aberrations caused by optical defects; especially, for the cloudy retinal image taken from cataract patient. Cataracts are the cause of cloudy vision where objects are obscured, blurred, and appear milky [1] [2]. This degraded image quality leads to incorrect diagnosis or delayed treatment. In this paper, a sharpness quality index is proposed for measuring and grading the color retinal images.

There are three categories of image quality measures: (1) full-reference approaches [3] [4], (2) reduced-reference approaches [5]; and (3) no-reference approaches [6] [7] [8] [9]. Full and reduced-reference approaches need the reference

image for assessing the quality of the distorted image. Unfortunately, in retinal image acquisition, the reference images are not available. In this case, the no-reference approach suits best.

No-reference retinal image quality assessment (RIQA) algorithms compute a numeric quality index that is related to the visibility of the anatomical details in the retinal image. It has been conducted by many researchers. Crété-Roffet *et al.* [7] proposed a no-reference perceptual blur metric by measuring the relative difference of the luminance variation between the input image and the image blurring version, which is achieved by convolving the input image with a low-pass filter. The more an image is blurred the less relative variation there is. Bahrami and Kot [8] proposed a no-reference image sharpness quality assessment by using a standard deviation of weighted maximum local variation (MLV) distribution to measure sharpness. However, the both quality assessment methods could not use to order the sharpness quality from the best to poor quality.

Recently, wavelet transform has been applied in most applications, such as steganography [10] and data compression [11] [12], especially in RIQA algorithms. Nirmala *et al.* [13] proposed a wavelet weighted blood vessel distortion to measure the green channel for quantification of the diagnostic information loss. The small and large blood vessels can be easily detected at levels 2 and 3 of the multiresolution wavelet filter process. However, this measure is not suitable for the cloudy retinal image of patients with a cataract.

Abdel-Hamid *et al.* [9] proposed a no-reference RIQA to assess the sharpness of the retinal images by employing the wavelet entropy [14]. The quality index (Q_r) is calculated by dividing the entropy of the detail sub-bands, which is equivalent to the information of image sharpness, by the wavelet entropy of the approximation sub-bands, which is equivalent to the information of image background. Next, an image homogeneity parameter was considered to account for reduced image quality due to the nonvisible structures in the adequately illuminated regions of the retinal image. However, the border region between the region of interest (ROI) of retinal image and its

black background leads to a problem through incorrect measurements.

This paper is motivated by the method of Abdel-Hamid *et al.* to overcome the drawbacks, it might be not correct order the image quality in HRF dataset. We study to design a quality index, which could sort the image quality of the dataset by the proposed index with corresponding to human vision system. The proposed index is developed to measure both the contrast and sharpness. Our image quality index is more consistent with human visual perception, and it could outperform the Abdel-Hamid *et al* method.

The paper proceeds as follows: the image database is introduced in Section II. The proposed method is described in Section III, our experimental results appear in Section IV, and discussion in Section V. Finally, the last paragraph introduces the main conclusions drawn.

II. Materials

A high-resolution fundus (HRF) image database [15] is applied to this work. The dataset images are captured with 18 image pairs of the same eye from 18 human subjects using a Canon CR-1 fundus camera with the Field of View (FOV) of 45°. For each pair, the quality of one image is good sharpness, whereas another is poor with slight blurs on the blood vessel and thus the image acquisition normally had to be repeated. Both bad and good images share approximately the same field of view. Therefore, the dataset images used for evaluation contain 18 bad and 18 good quality images.

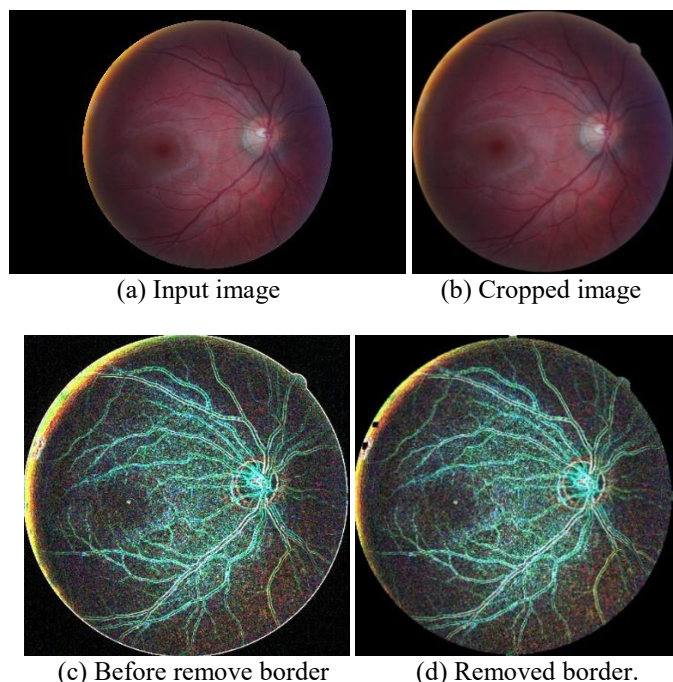


Fig. 1 Preprocessing step consisting of cropping ROI, and removing the border regions between the ROI and background.

III. The proposed method

The high-quality retinal images are suitable for diagnosis. It is easy to see the lesions that occur in the photographs. RIQA algorithm is therefore required in order to

evaluate the image quality. Our RIQA method was designed to select the high-quality images. The proposed method consists of two steps. The first step supplies to preprocess the images consisting of cropping the ROI and removing the border between a background and the ROI as seen in Fig. 1. In Fig. 1, the input image has the size 3456×5184 pixels, after cropping the size of image is 3260×3266 pixels. From our study, the border between ROI and the background region appears after wavelet decomposition process as seen in Fig. 1(c). In our case, the border is noise, which is a cause to the method of Abdel-Hamid *et al.* unable to sort image quality of the dataset. Thus, in our method the border of all sub-band is removed as shown in Fig. 1(d).

In the second step, the quality index employed wavelet transform to objectively assess the sharpness of anatomical structures of the retinal images. Multiresolution Daubechies (db2) wavelet filter is used to decompose the input image into horizontal (H) and vertical (V) detail sub-bands corresponding with the sharpness information of image foreground, and an approximation sub-band (A) corresponding with the image background.

The proposed quality index, $Q_{sharpness}$, can be calculated by dividing the entropy of H and V by A at level 4 as given:

$$Q_{sharpness} = \frac{E(H)+E(V)}{E(A)} \quad (1)$$

where $E(H)$, $E(V)$, and $E(A)$ are the wavelet Shannon entropies of the horizontal, vertical and approximation sub-bands, respectively. The wavelet Shannon Entropy for each sub-band in Equation (1) is calculated using the following equation:

$$E(C) = |\sum_{i=1}^N \log(C_i^2)| \quad (2)$$

where N is the number of coefficients in the wavelet sub-band, C is the wavelet coefficient of Db2 at level 4 and C_i is the wavelet coefficient having an index i within the respective sub-bands.

To show that level 4 of wavelet multiresolution decomposition with db2 suits to measure the image sharpness, especially the cloudy retinal image, the image 1_bad.jpg from the HRF dataset is decomposed as shown in Fig. 2. This image is obscured and appears milky. Fig. 2 demonstrates the output results derived from each level of multi-scale Daubechies wavelet transform decomposition process. At level 1, the input image was first downsized by 2 and then decomposed with db2 resulting in an approximation sub-band A_1 , and three detailed sub-bands, the horizontal H_1 , vertical V_1 , and diagonal D_1 . By using the same process in level 1, all obtained sub-band outputs C_i , can be expressed as $C_i = \{A_i, H_i, V_i, D_i\}$ where i is the scale level from 1 to 5.

As mentioned in the introduction section, the study by Nirmala *et al.* [13] suggested that the small and large blood vessels can be easily seen at the second and third level. However, their study is not comprehensive in blurred regions that appear in the cloudy retinal images.

By wavelet multiresolution decomposition with db2 in Fig. 2, the blurred regions in the partial image appeared clearly at H_4 and H_5 . Those regions reduce the image sharpness and lead to the loss of the necessary anatomical structure details

required for accurate interpretation. To determine the information quality of H_4 (204×204 resolution) and H_5 with (102×102 resolution), the H_4 and H_5 of Fig. 2 were magnified as shown in Fig. 3.

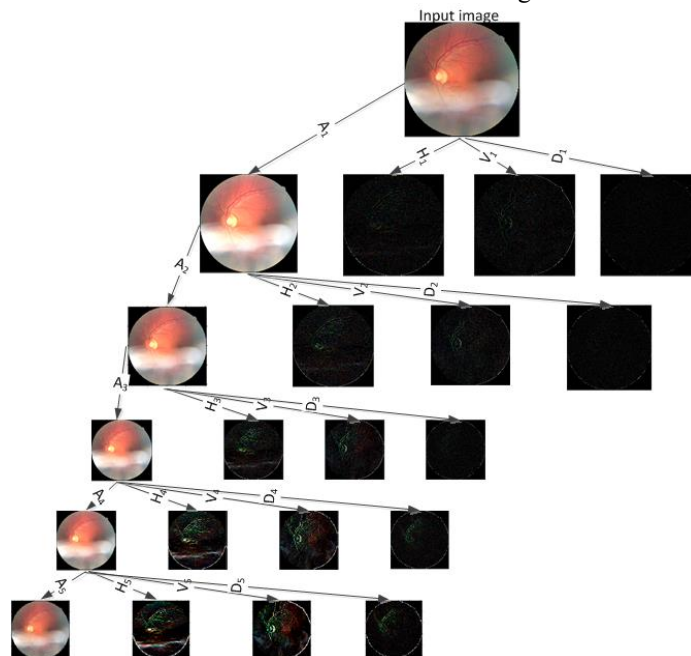


Fig. 2 Tree diagram of wavelet multiresolution decomposition with db2 from level 1 to 5.

From Fig. 3, it is clearly seen that the blood vessel in H_4 provides much more details and continuity than H_5 . This result shows that the coefficients of H_4 sub-band has comparatively higher impact than H_5 sub-band.

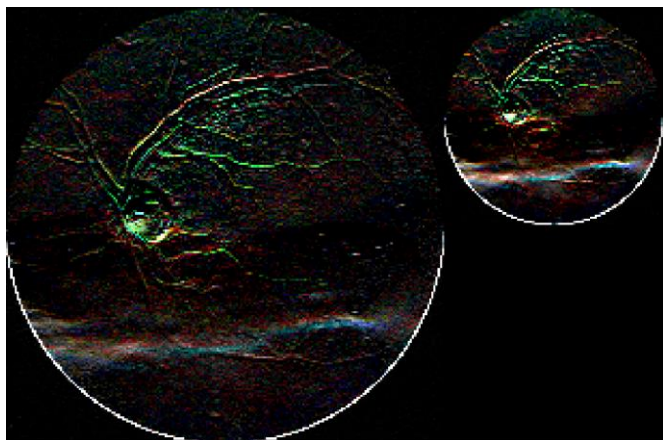


Fig. 3 Comparison of the detail information of H_4 and H_5 .

Moreover, the horizontal detail sub-band of blood vessels is greater than the vertical, therefore, the information in H_4 suits the most to measure the image sharpness. Fig. 4 shows a comparison of H_4 between the blurred and sharp images. The H_4 corresponding to Fig. 4 (a) and (b) are shown in (c) and (d), respectively.

Fig. 4 indicates that the H_4 sub-band provided an obvious difference between the blurred and sharp image. This

is the main reason why the proposed quality index calculated the entropy of approximation and detailed sub-bands at level 4.

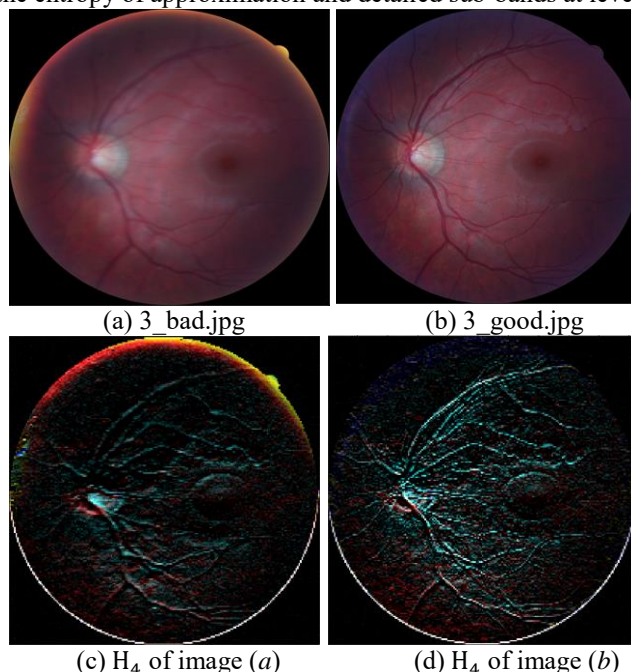


Fig. 4 Level 4 horizontal detail sub-band: H_4 of blurry (a, c) and sharp (b, d) retinal image from HRF.

IV. Experimental Results

To evaluate the performance of our method, all images from the HRF dataset are used to compute the sharpness index

with $Q_{sharpness}$ and Abdel-Hamid *et al.* method, Q_r . Table 1 shows $Q_{sharpness}$ and Q_r values which are sorted by descending order. The first three columns comprise the order, filename, and sharpness index from the proposed method, respectively, while the last three columns are formulated by the

Abdel-Hamid *et al.* method. To compare the characteristics of the indexes, Fig. 5 depicts the graph of each image pair: bad and good from Table 1. Considering the line graphs of $Q_{sharpness}$, the quality index of good images remains constantly above all bad images.

Table 1 Comparison of $Q_{sharpness}$ and Q_r value by using HRF dataset.

The proposed method			Abdel-Hamid <i>et al.</i> method [16] [17]		
Order	Filename	$Q_{sharpness}$	Order	Filename	Q_r
1	12_good.JPG	0.6588	1	2_good.JPG	0.1864
2	18_good.JPG	0.6559	2	5_good.JPG	0.0910
3	9_good.JPG	0.6559	3	16_good.JPG	0.0850
4	17_good.JPG	0.6446	4	12_good.JPG	0.0843
5	8_good.JPG	0.6446	5	17_good.JPG	0.0706
6	11_good.JPG	0.6384	6	8_good.JPG'	0.0706
7	16_good.JPG	0.6373	7	12_bad.JPG	0.0700
8	3_good.JPG	0.6340	8	5_bad.JPG	0.0690
9	4_good.JPG	0.6315	9	11_bad.JPG	0.0687
10	15_good.JPG	0.6238	10	18_bad.JPG	0.0683
11	13_good.JPG	0.6094	11	18_good.JPG	0.0655
12	5_good.JPG	0.6074	12	9_good.JPG	0.0655
13	14_good.JPG	0.6012	13	16_bad.JPG	0.0626
14	10_good.JPG	0.5940	14	13_good.JPG	0.0624
15	7_good.JPG	0.5921	15	11_good.JPG	0.0622
16	17_bad.JPG	0.5693	16	14_good.JPG	0.0605
17	5_bad.JPG	0.5682	17	9_bad.JPG	0.0590
18	7_bad.JPG	0.5679	18	15_good.JPG	0.0561
19	12_bad.JPG	0.5674	19	15_bad.JPG	0.0521
20	18_bad.JPG	0.5513	20	10_good.JPG	0.0495
21	8_bad.JPG	0.5338	21	14_bad.JPG	0.0453
22	4_bad.JPG	0.5283	22	8_bad.JPG	0.0452
23	1_good.JPG	0.5264	23	13_bad.JPG	0.0443
24	9_bad.JPG	0.5139	24	2_bad.JPG	0.0434
25	11_bad.JPG	0.5119	25	3_good.JPG	0.0400
26	14_bad.JPG	0.4854	26	17_bad.JPG	0.0378
27	15_bad.JPG	0.4804	27	1_good.JPG	0.0323
28	13_bad.JPG	0.4718	28	4_bad.JPG	0.0302
29	16_bad.JPG	0.4629	29	7_good.JPG	0.0287
30	3_bad.JPG	0.4557	30	10_bad.JPG	0.0270
31	10_bad.JPG	0.4407	31	6_good.JPG	0.0259
32	1_bad.JPG	0.4261	32	6_bad.JPG	0.0251
33	2_good.JPG	0.4221	33	7_bad.JPG	0.0246
34	6_good.JPG	0.3953	34	1_bad.JPG	0.0172
35	6_bad.JPG	0.3783	35	4_good.JPG	0.0167
36	2_bad.JPG	0.3141	36	3_bad.JPG	0.0122

When considering line graphs of Q_r , the graph lines of good and bad images have interfered. The results

accumulated in Table 1, appear that the proposed method performs better than the Abdel-Hamid *et al.* method as most

good images ranked higher and when compare with the same x images, there is no x_bad.jpg images with the $Q_{sharpness}$ values higher than x_good.jpg images. In contrast, some x_bad.jpg images highlighted in bold in Table 1, give higher

Q_r values than x_good.jpg such as the Q_r values of 4_good.jpg in the 35th order (0.0167) is less than Q_r values of 4_bad.jpg (0.0302).

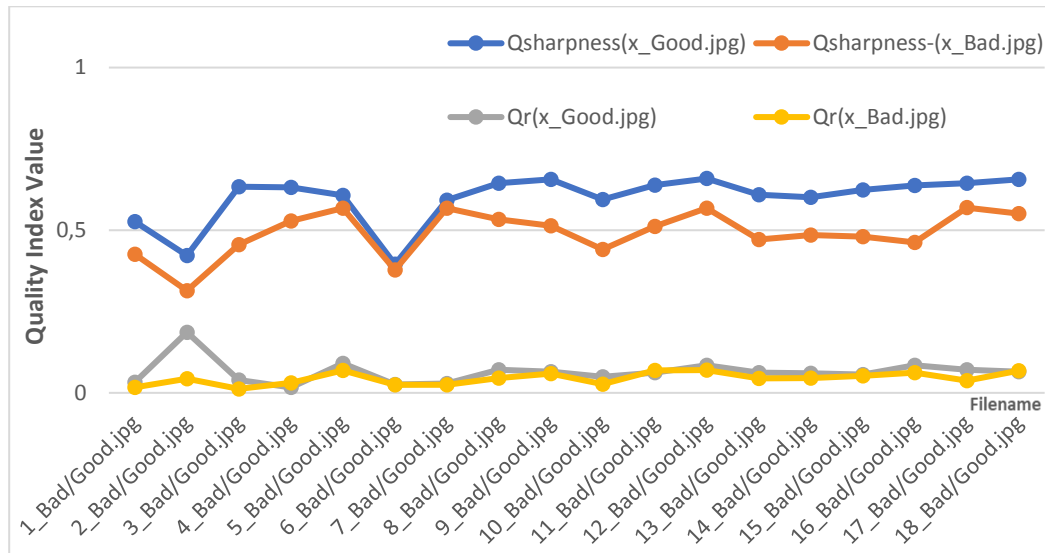


Fig. 5 The line graph of the quality index between the proposed and Abdel-Hamid *et al.* method for the same pair of good and bad images.

Fig. 6 shows the comparison of $Q_{sharpness}$ and Q_r for the same pair of images, 4_good.jpg and 4_bad.jpg with $Q_{sharpness} = 0.6315$ and 0.5283 while $Q_r = 0.0167$ and 0.0302 , respectively. It can be seen that 4_good.jpg resulted in a greater $Q_{sharpness}$ value than the 4_bad.jpg image while the

4_good.jpg image presented a smaller Q_r value less than 4_bad.jpg. These results show that the proposed method provides more appropriate order than the Abdel-Hamid *et al.* method.

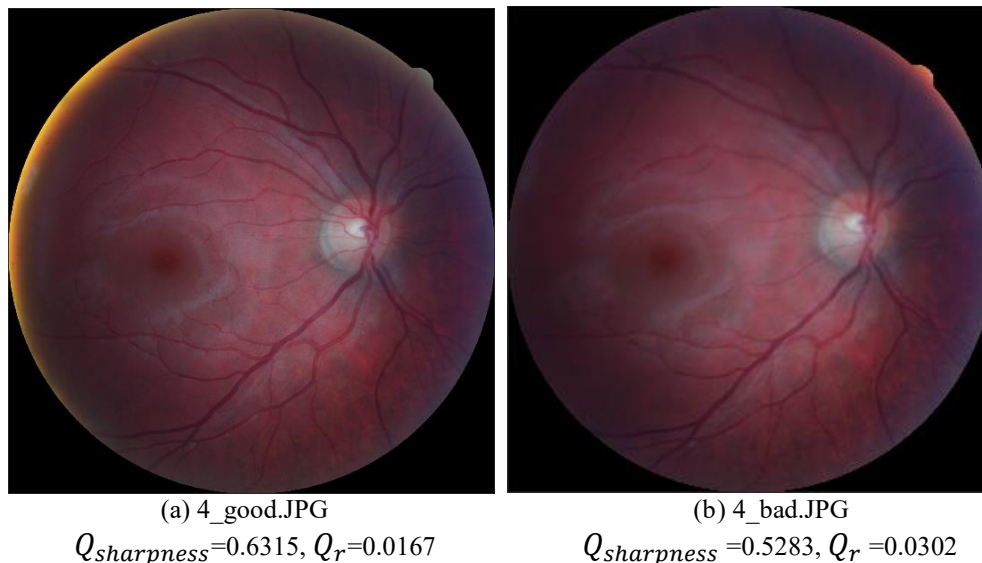
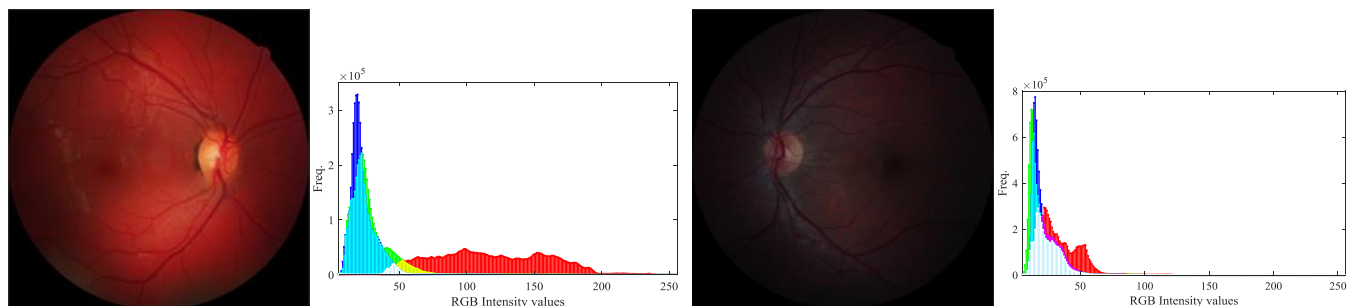


Fig. 6 Sharpness index comparison between $Q_{sharpness}$ and Q_r .

Fig. 7 highlights the images 12_good.JPG and 2_good.JPG from the HRF dataset with their image histograms where image 12_good.JPG reaches the maximum quality index of the proposed method ($Q_{sharpness}=0.6588$) and image 2_good.JPG reaches the maximum quality index of the Abdel-

Hamid *et al.* method ($Q_r=0.1864$). Although the image 2_good.JPG image provides great sharpness its contrast is quite low as seen in the image histogram. In addition, the image with low contrast should not be used for enhancement because the enhancement results in undesirable image tone and color

balance. As a result, the image with low contrast should not have a high-quality index.



(a) 12_good.JPG

$$Q_{sharpness}=0.6588 \text{ [Order=1]}$$

$$Q_r=0.0843 \text{ [Order = 4]}$$

(b) 2_good.JPG

$$Q_{sharpness}=0.4221 \text{ [Order =33]}$$

$$Q_r=0.1864 \text{ [Order = 1]}$$

Fig. 7 Images with their image histograms that reached the maximum $Q_{sharpness}$ and Q_r .

Fig. 8 and Fig. 9 illustrated some photographs for visualize evaluation, which sorted from high to low quality indexes by using Q_r and $Q_{sharpness}$, respectively. The photographs were selected by the same order at 1, 8, 15, 22, 29, and 36 as seen in Table 1. As seen in Fig. 8, the sequence of

images sorted by the Q_r value have several conflicts when comparing with the sequence that are sorted by $Q_{sharpness}$ in Fig. 9.

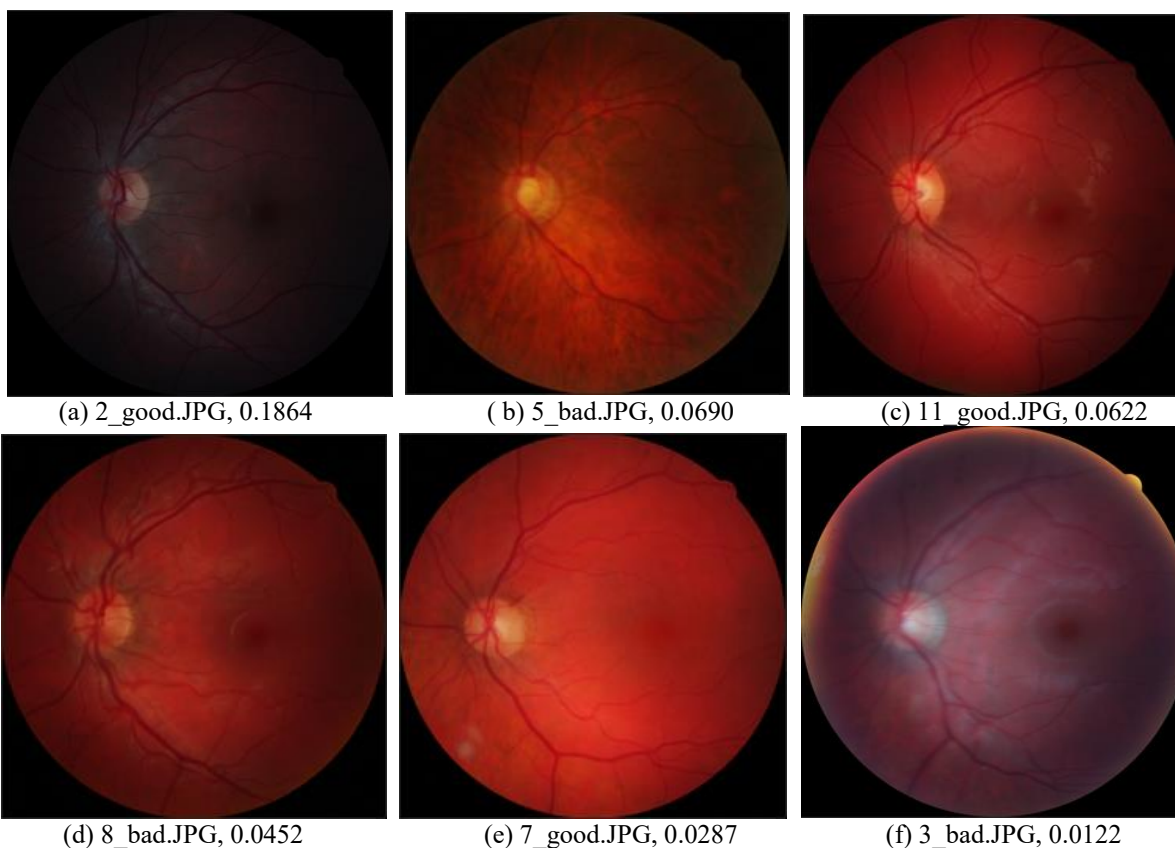


Fig. 8 Example of image sequence sorted by Q_r .

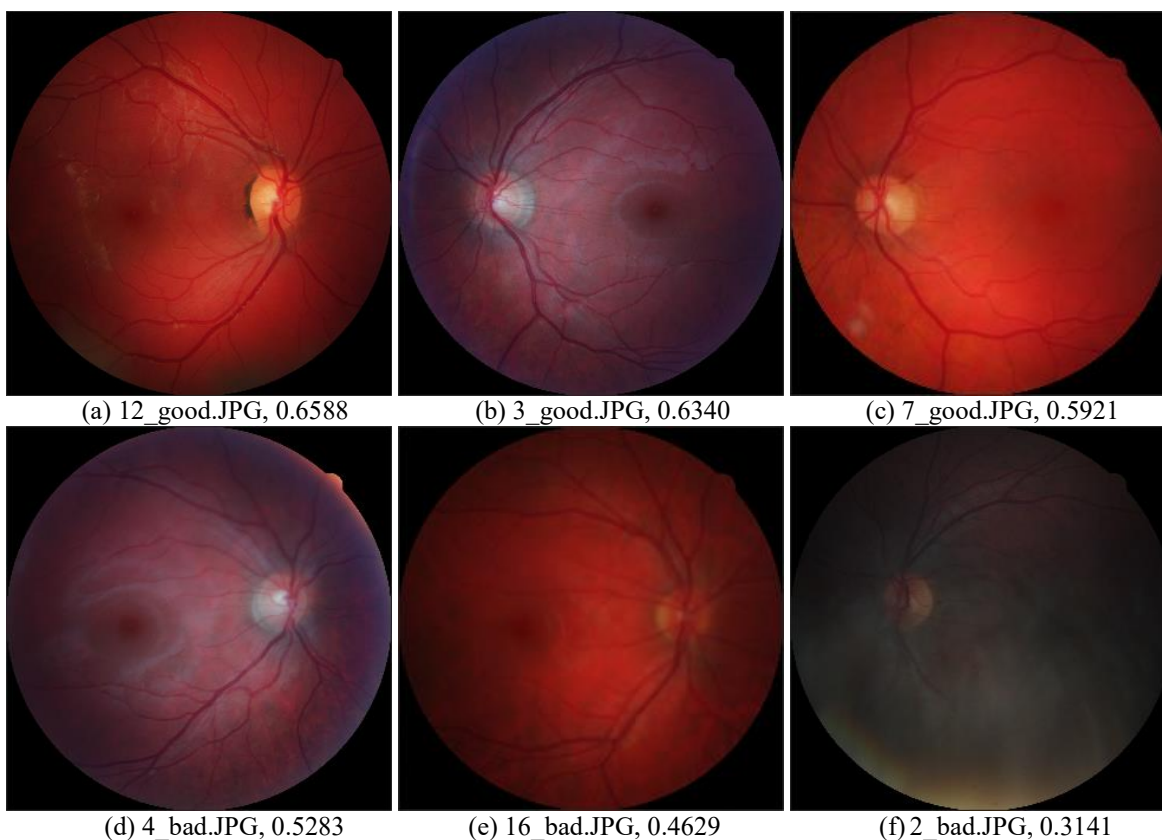


Fig. 9 Example of image sequence sorted by $Q_{sharpness}$.

However, three good-quality images in Fig. 10 obtained a metric score lower than 0.5921. Although those three images are classified as good quality image [15] perception-wise, they look unsatisfactory and show low correlation with

human evaluations. Fig. 10 (a) appears an edge haze around the circular border which directly affect the image sharpness while many dark regions in Fig. 10 (b) and (c) are caused by non-uniform illumination.

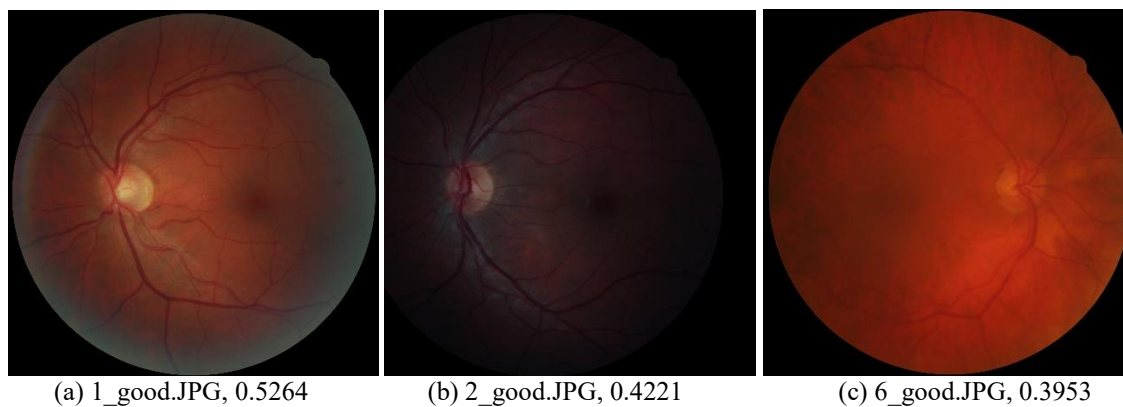


Fig. 10 Example of good quality images with low $Q_{sharpness}$ value.

V. Discussion

The $Q_{sharpness}$ index could be used in the quality evaluation procedure. Good quality images are accepted for further diagnosis by ophthalmologists, while bad quality images are rejected, and re-imaging is required. From Table1, images from order one to fifteen are good quality images. Hence, the minimum $Q_{sharpness}$ value for a good quality image should be 0.6. As seen from Fig. 10, when $Q_{sharpness}$ less than 0.6, those regions obscure the anatomical structures in the image. All

artifacts in those three images decrease the quality of image [18] [19] and affect to the $Q_{sharpness}$ index.

VI. Conclusion

A no-reference wavelet-based quality index was proposed to measure the sharpness of the color retinal images. The sharpness index is deduced from the ratio between the structural image in horizontal and vertical details and the blurriness in approximation sub-band, which is calculated by db2 at the 4th

level with the energy entropy. The index can measure the image quality as demonstrated in the results. Good and bad images could be compared as shown in Fig. 5; on the other hand, image quality could be arranged as reported in Table I. From the quality arrangement by our index, the retinal photographs can be used for diagnosis when the $Q_{\text{sharpness}}$ value is greater than or equal to 0.6.

References

- [1] A. M. Abdul-Rahman, T. Molteno and A. C. Molteno, "Fourier analysis of digital retinal images in estimation of cataract severity," *Clinical and Experimental Ophthalmology*, vol. 36, pp. 637-645, 2008.
- [2] M. D. Abramoff, M. K. Garvin and M. Sonka, "Retinal imaging and image analysis," *IEEE Rev Biomed Eng.*, vol. 3, p. 169-208, 2010.
- [3] Z. Wang and A. C. Bovik, "Mean squared error: love it or leave it? A new look at signal fidelity measures," *Signal Processing Magazine*, vol. 26, pp. 98-117, 2009.
- [4] H.-S. Han, D.-O. Kim and R.-H. Park, "Structural information-based image quality assessment using LU factorization," *IEEE Transactions on Consumer Electronics*, vol. 55, pp. 165-171, 2009.
- [5] Q. Li and Z. Wang, "General-purpose reduced-reference image quality assessment based on perceptually and statistically motivated image representation," in *ICIP 2008*, 2008.
- [6] K. Panetta, C. Gao and S. Agaian, "No reference color image contrast and quality measures," *IEEE Transactions on Consumer Electronics*, vol. 59, pp. 643-651, 2013.
- [7] F. Crete, T. Dolmiere, P. Ladret and M. Nicolas, "The Blur Effect: Perception and Estimation with a New No-Reference Perceptual Blur Metric," in *Proc. SPIE 6492, Human Vision and Electronic Imaging XII*, 2007.
- [8] K. Bahrami and A. C. Kot, "A Fast Approach for No-Reference Image Sharpness Assessment Based on Maximum Local Variation," *IEEE Signal Processing Letters*, vol. 21, no. 6, pp. 751-755, 2014.
- [9] L. Abdel-Hamid, A. El-Rafei and G. Michelson, "No-reference quality index for color retinal images," *Computers in Biology and Medicine*, vol. 90, pp. 68-75, 2017.
- [10] S. Dutta and K. Saini, "Securing Data: A Study on Different Transform Domain Techniques," *WSEAS TRANSACTIONS on SYSTEMS and CONTROL*, vol. 16, pp. 110-120, 2021.
- [11] Z. Gao and Y. F. Zheng, "Quality constrained compression using DWT-based image quality metric," *IEEE Transactions on Circuits and Systems for Video Technology*, vol. 18, no. 7, p. 910-922, 2008.
- [12] K. P and J. M., "An Integrated Data Compression using Wavelet and Neural Networks for Power Quality Disturbances," *WSEAS Transactions on Computer Research*, vol. 7, pp. 9-22, 2019.
- [13] S. Nirmala, S. Dandapat and P. Bora, "Wavelet weighted blood vessel distortion measure for retinal images," *Biomedical Signal Processing and Control*, vol. 4, no. 5, pp. 282-291, 2010.
- [14] R. R. Coifman and M. V. Wickerhauser, "Entropy-based Algorithms for best basis selection," *IEEE Trans. Inf. Theory*, vol. 38, no. 2, p. 713-718, 1992.
- [15] T. Köhler, A. Budai, M. Kraus, J. Odstrcilik, G. Michelson and J. Hornegger, "Automatic no-reference quality assessment for retinal fundus images using vessel segmentation," in *Proceedings of the 26th IEEE International Symposium on Computer-Based Medical Systems*, Porto, Portugal, 2013.
- [16] L. Abdel-Hamid, A. El-Rafei and G. Michelson, "No-reference quality index for color retinal images," *Computers in Biology and Medicine*, vol. 8, pp. 68-75, 2017.
- [17] L. Abdel-Hamid, A. El-Rafei, S. El-Ramly, G. Michelson and J. Hornegger, "Retinal image quality assessment based on image clarity and content," *J. Biomed. Opt. SPIE*, vol. 21, no. 9, pp. 1-17, 2016.
- [18] R. C. Gonzalez and R. E. Woods, *Digital Image Processing third edition*, Pearson Prentice Hall, 2009.
- [19] J. Lin, L. Yu, Q. Weng and X. Zheng, "Retinal Image Quality Assessment For Diabetic," *Multimedia Tools and Applications*, vol. 79, pp. 16137-16199, 2020.

AUTHOR CONTRIBUTIONS:

Preecha Vonghirandecha organized the manuscript and executed the experiment.

Patama Bhurayanontachai was responsible for the experimental design and assessment.

Supaporn Kansomkeat was responsible for the algorithm testing.

Sathit Intajag proposed the algorithm, carried out the simulation, and executed the experiment.

Creative Commons Attribution License 4.0 (Attribution 4.0 International, CC BY 4.0)

This article is published under the terms of the Creative Commons Attribution License 4.0

https://creativecommons.org/licenses/by/4.0/deed.en_US